Measurements of higher order noise correlations in a quantum dot with a finite bandwidth detector

S. Gustavsson,* R. Leturcq, T. Ihn, and K. Ensslin
Solid State Physics Laboratory, ETH Zürich, CH-8093 Zürich, Switzerland

M. Reinwald and W. Wegscheider
Institut für experimentelle und angewandte Physik, Universität Regensburg, Germany
(Dated: February 6, 2008)

We present measurements of the fourth and fifth cumulants of the distribution of transmitted charge in a tunable quantum dot. We investigate how the measured statistics is influenced by the finite bandwidth of the detector and by the finite measurement time. By including the detector when modeling the system, we use the theory of full counting statistics to calculate the noise levels for the combined system. The predictions of the finite-bandwidth model are in good agreement with measured data.

PACS numbers:

Current fluctuations in mesoscopic systems have been extensively studied due to the extra information they give in comparison to measurements of the mean current [1]. The focus has traditionally been on investigations of the shot-noise, which for classical systems arises due to the discreteness of the electron charge. The theory of full counting statistics (FCS) was introduced as a new way of examining current fluctuations [2]. With the FCS, fluctuations are studied by counting the number of electrons that pass through a conductor within a fixed period of time. This gives direct access to the probability distribution function $p_{t_0}(N)$, which is the probability that N electrons are transferred within a time interval of length t_0. From the distribution function, not only the shot noise but also correlations of higher order can be calculated.

The third moment of a tunneling current has been shown to be independent of the thermal noise [3, 4], thus making it a potential tool for investigating electron-electron interactions even at elevated temperatures. Higher order moments in strongly interacting systems are predicted to depend heavily on both the conductance [5] and on the internal level structure [6] of the system. Determining higher order moments may therefore give a more complete characterization of the electron transport process. This can be of importance for realizing measurements of electron correlation and entanglement effects in quantum dots [7, 8].

Experimentally, the third moment of the current distribution function has been measured for a tunnel junction [9] as well as for a single quantum dot (QD) [10, 11] and a double QD [3]. In quantum optics, higher order moments are routinely measured in order to study entanglement and coherence effects of the electromagnetic field [12]. Here, we set out to measure the fourth and fifth cumulant of the distribution function for charge transport through a QD.

In general, experimental measurements of FCS for electrons are difficult to achieve due to the need of a sensitive, high-bandwidth detector capable of resolving individual electrons [13, 14, 15]. However, a more fundamental complication with the measurements is that most forms of the FCS theory assume the existence of (1) a detector with infinite bandwidth and (2) infinitely long data traces. Since no physical detector can fulfill these requirements, every experimental realization of the FCS will measure a distribution which is influenced by the properties of the detector. Here, we investigate how the violation of the two assumptions modifies the measured statistics. By including the detector in the model, the FCS for the combined QD-detector system can be calculated. This model can explain the results for higher order cumulants measured with a finite bandwidth detector.

The sample consists of a QD [dotted circle in the inset of Fig. 1(b)] with a nearby quantum point contact (QPC) used for reading out the charge state of the QD [16]. The structure was fabricated using scanning probe lithography [17] on a GaAs/$Al_{0.3}Ga_{0.7}$As heterostructure with a two-dimensional electron gas 34 nm below the surface. The gates G_1 and G_2 are used to tune the height of the tunneling barriers connecting the dot to source and drain leads, while the P-gate is used to keep the conductance through the QPC in a regime where the sensitivity to changes in its electrostatic potential is maximal. All measurements were performed in a dilution refrigerator with a base temperature of 20 mK. The electronic temperature extracted from the width of Coulomb blockade resonances measured in the low bias regime [18] was 190 mK.

Due to the electrostatic coupling between the QD and the QPC, the addition of an extra electron on the dot will cause a change in the QPC conductance. By performing time-resolved measurements of the current through the QPC, tunneling of single electrons can be detected in real-time [14, 19, 20]. In this experiment, the QPC was voltage biased with $V_{QPC} = 250\ \mu V$. The current signal

*Electronic address: simongus@phys.ethz.ch

was sampled at 100 kHz, software filtered at 4 kHz using a 8th order Butterworth filter and finally resampled at 20 kHz to keep the amount of data manageable.

To measure the higher cumulants for the current through the QD, one has to generate the experimental probability density function $p_{t_0}(N)$. This is done by splitting a time trace of length T into $m = T/t_0$ intervals and counting the number of electrons entering the dot within each interval. The cumulants are then calculated directly from the distribution function. In a previous experiment on a similar system the second and third cumulants were measured [10]. To extend the analysis to higher cumulants, it is necessary to increase the length of the time traces in order to collect more statistics. Here, we present cumulants extracted from time traces of length $T = 10$ minutes. The quality of the data allows to measure up to the fifth cumulant, which is two orders higher than reported in previous experiments [3, 9, 10].

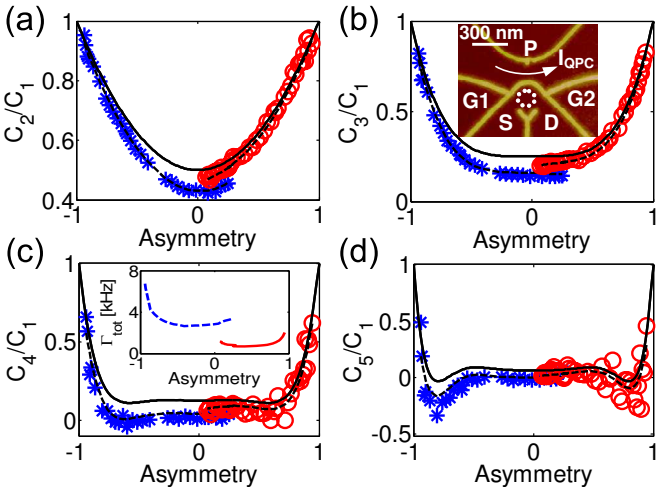

FIG. 1: (a-d) Normalized cumulants C_n/C_1 versus dot asymmetry, $a = (\Gamma_{in} - \Gamma_{out})/(\Gamma_{in} + \Gamma_{out})$. The solid lines are theoretical predictions assuming a perfect detector, $C_2/C_1 = (1 + a^2)/2$, $C_3/C_1 = (1 + 3a^4)/4$, $C_4/C_1 = (1 + a^2 - 9a^4 + 15a^6)/8$ and $C_5/C_1 = (1 + 30a^4 - 120a^6 + 105a^8)/16$. The dashed lines show the cumulants calculated from the model defined by Eq. (1) in the text. The inset in (b) shows the quantum dot with integrated charge read-out used in the experiment. The inset in (c) shows the variation of the total tunneling rate $\Gamma_{tot} = \Gamma_{in} + \Gamma_{out}$ for the different measurement points.

The results are shown in Fig. 1, where we plot the normalized cumulants for different values of the asymmetry of the tunneling rates, $a = (\Gamma_{in} - \Gamma_{out})/(\Gamma_{in} + \Gamma_{out})$. Here, Γ_{in} and Γ_{out} are the rates for tunneling into and out of the dot, respectively. The asymmetry is tuned by shifting the voltage on gate G_1 by an amount ΔV and at the same time applying a compensating voltage $-\Delta V$ on gate G_2. With the two gates having a similar lever arm on the dot, the electrochemical potential of the QD remains at the same level, but the height of the tunneling barriers between the dot and the source and drain leads will change. Doing so, we could tune the asymmetry from $a = -0.94$ to $a = +0.25$ while still keeping both tunneling rates within the measurement bandwidth and avoiding charge rearrangements. To get data for the full range of asymmetry, we did a second measurement at a different gate voltage configuration. For the second set of data, the asymmetry was tuned from $a = 0.07$ to $a = 0.93$. The stars and the circles in Fig. 1 represent data from the two different sets of measurements. The measurements were performed with a QD bias of $V_{bias} = 2.5$ mV, with the electrochemical potential of the dot far away from the Fermi levels of the source and drain leads. This is to ensure that tunneling due to thermal fluctuations is sufficiently suppressed [10].

The solid lines in Fig. 1 depict the theoretical predictions calculated from a two-state model [21]. The analytical expressions are given in the figure caption. The higher cumulants show a complex behavior as a function of the asymmetry, with local minima at $a = \pm 0.6$ for C_4/C_1 and at $a = \pm 0.8$ for C_5/C_1. The fifth cumulant even becomes negative for some configurations. The experimental data qualitatively agrees with the theory, but for small values of the asymmetry there are deviations from the expected behavior. The deviations are stronger for the first set of data (stars). Since the tunneling rates in the first measurement was about a factor of three higher than in the second measurement [see inset of Fig. 1(c)], we suspect the finite bandwidth of the detector to be a possible reason for the discrepancies.

Recently, Naaman et al. [22] pointed out that measurements of the transition rates of a Poisson two-state system using a finite bandwidth detector always leads to an underestimate of the rates. To determine the rates correctly, the detection rate Γ_{det} of the detector must be taken into account. In the low-bias, weak coupling Coulomb blockade regime, the QD can be modeled as a Poisson two-state system. The two states correspond to zero or one excess electron on the dot, and the transitions between the two states occur whenever an electron tunnels into or out of the dot. The probability distribution for the times needed for an electron to tunnel into or out of the QD follows the exponential $p_{in/out}(t) = \Gamma_{in/out} \exp(-\Gamma_{in/out}\, t)$ [19].

An example of a probability distribution taken from measured data is shown in Fig. 2(a). The long-time behavior is exponential, but for times $t < 100$ μs there is a sharp decrease in the number of counts registered by the detector. From the figure, we can estimate τ_{det}, which is the average time it takes for the detector to register an event. We find $\tau_{det} = 70$ μs, giving a detection rate of $\Gamma_{det} = 1/\tau_{det} = 14$ kHz. Note that the detection rate Γ_{det} does not only depend on the measurement bandwidth but also on the signal-to-noise ratio of the detector signal as well as the redundancy needed to minimize the risk of detecting false events [23]. All tunneling rates presented in the following have been extracted from distributions such as the one shown in Fig. 2(a), using the methods described in Ref. [22] with $\Gamma_{det} = 14$ kHz.

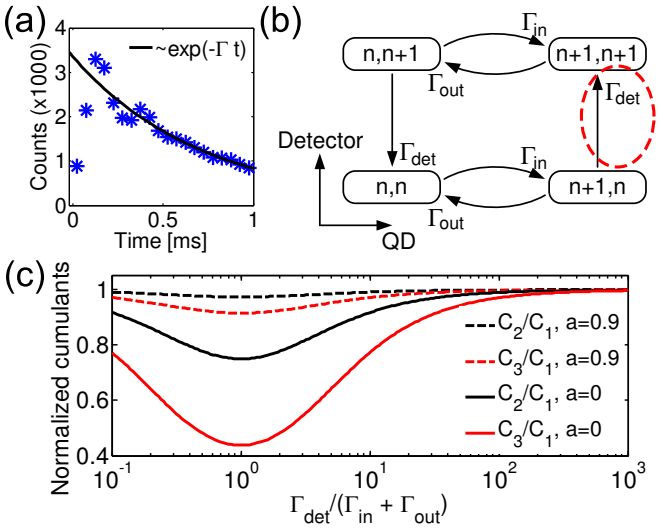

FIG. 2: (a) Probability density of time needed for an electron to tunnel into the dot. Note the sharp decrease in counts for $t < 100$ μs due to the finite bandwidth of the detector. The black curve is a long-time exponential fit with $\Gamma = 1.39$ kHz. (b) Model for the dot-detector system. A state (n, m) corresponds to n electrons on the dot while the detector at the same time is measuring m electrons. (c) Higher cumulants versus relative detection bandwidth $\Gamma_{\rm det}/(\Gamma_{\rm in} + \Gamma_{\rm out})$, calculated from the model in (b). The cumulants are normalized to the results from the infinite-bandwidth case. The influence of the finite bandwidth is maximal when the asymmetry $a = (\Gamma_{\rm in} - \Gamma_{\rm out})/(\Gamma_{\rm in} + \Gamma_{\rm out})$ is zero.

The finite bandwidth will also influence the FCS measured by the detector. Following the ideas of Ref. [22], we account for the finite bandwidth by including the states of the detector in the model. Figure 2(b) shows the four possible states of the combined dot-detector model. The state $(n+1, n)$ refers to a situation where there are $n+1$ electrons on the dot, while the detector at the same time reads n electrons. The transition from the state $(n+1, n)$ to the state $(n+1, n+1)$ occurs when the detector registers the electron. This process occurs with the rate of the detector, $\Gamma_{\rm det}$.

To calculate the FCS for the QD-detector system, we write the master equation $\dot{P} = M\,P$, with $P = [(n,n),(n+1,n),(n,n+1),(n+1,n+1)]$ and

$$M_\chi = \begin{pmatrix} -\Gamma_{\rm in} & \Gamma_{\rm out} & \Gamma_{\rm det} & 0 \\ \Gamma_{\rm in} & -(\Gamma_{\rm out}+\Gamma_{\rm det}) & 0 & 0 \\ 0 & 0 & -(\Gamma_{\rm in}+\Gamma_{\rm det}) & \Gamma_{\rm out} \\ 0 & \Gamma_{\rm det} * e^{i\chi} & \Gamma_{\rm in} & -\Gamma_{\rm out} \end{pmatrix}. \quad (1)$$

In the above matrix, we have included the counting factor $e^{i\chi}$ at the element where the detector registers an electron tunneling into the dot [see dashed circle in Fig. 2(b)]. The statistics obtained in this way relates directly to what is measured in the experiment. Using the methods of Ref. [21], we calculate the first few cumulants for the above expression as a function of relative bandwidth $k = \Gamma_{\rm det}/(\Gamma_{\rm in} + \Gamma_{\rm out})$ and asymmetry $a = (\Gamma_{\rm in} - \Gamma_{\rm out})/(\Gamma_{\rm in} + \Gamma_{\rm out})$. The normalized second and third cumulants take the form

$$C_2/C_1 = \frac{1+a^2}{2} - \frac{k(1-a^2)}{2(1+k)^2}, \quad (2)$$

$$C_3/C_1 = \frac{1+3a^4}{4} - \frac{3k(1+k+k^2)}{4(1+k)^4} - \frac{6\,a^2k^2}{4(1+k)^4} + \frac{3\,a^4k(1+3k+k^2)}{4(1+k)^4}. \quad (3)$$

In Fig. 2(c) we plot the second and third cumulants from Eq. (2) and Eq. (3) for different values of asymmetry a and relative bandwidth k. The cumulants have been normalized to the values for the infinite bandwidth detector. With $\Gamma_{\rm det} \gg \Gamma_{\rm in} + \Gamma_{\rm out}$, the cumulants approach the infinite bandwidth result, as expected. However, even with $\Gamma_{\rm det} = 10(\Gamma_{\rm in}+\Gamma_{\rm out})$ and perfect symmetry ($a = 0$), the second cumulant deviates by almost 10% and the third cumulant by more than 20% from the perfect detector values. As the bandwidth is further decreased, the deviations grow stronger and reach a maximum as $\Gamma_{\rm det} = \Gamma_{\rm in}+\Gamma_{\rm out}$. With $\Gamma_{\rm det} \ll \Gamma_{\rm in}+\Gamma_{\rm out}$, the cumulants once again approach the perfect detector values. When the detector is much slower than the underlying tunneling process, it will only sample the average population of the two states. In this limit, the dynamics of the system does not interfere with the dynamics of the detector and we recover the correct relative noise levels. It should be noted that this is true only for the noise relative to the detected mean current. Since the detector will miss most of the tunneling events, the absolute values of both the current and the noise will be underestimated.

We have also performed the analysis for the fourth and fifth cumulants. We do not show the analytical expressions due to space limitations; however, the results corresponding to the experimental configuration are represented by the dashed lines in Fig. 1. Over the full range of bandwidth and asymmetry, we find that the noise detected with the finite bandwidth system is always lower than for the ideal detector case. The reduction can be qualitatively understood by considering the probability distribution $p_{t_0}(N)$. The finite bandwidth makes it less probable to detect fast events, meaning that the probability of detecting a large number of electrons within the interval t_0 will decrease more than the probability of detecting few electrons. This will cut the high-count tail of the distribution and thereby reduce its width (C_2) and its skewness (C_3). An interesting feature is that the cumulants calculated for a less symmetric configurations [$a = 0.9$ in Fig. 2(c)] show less influence of the finite bandwidth.

A second limitation of a general FCS measurement is the finite length of each time trace. In order to generate the experimental probability density function $p_{t_0}(N)$, the total trace of length T must be split into $m = T/t_0$ intervals, each of length t_0. Most FCS theories only predict results for the case $t_0 \gg 1/\Gamma$, where Γ is a typical transition rate of the system. In the experiment, it is favorable

to make t_0 as short as possible in order to increase the number of samples $m = T/t_0$. This will improve the quality of the distribution and help to minimize statistical errors.

The condition $t_0 \gg \Gamma$ is imposed by the approximation that the cumulant generating function (CGF) $S(\chi)$ for $p_{t_0}(N)$ only depends on the lowest eigenvalue $\Lambda_{\min}$ of the master equation matrix M_χ, with $S(\chi) = -t_0\Lambda_{\min}$. A FCS valid for finite t_0 must include all eigenvalues and eigenvectors of M_χ [21] . The corresponding expression is

$$\exp[S(\chi)] = \langle q_0|p^{(n)}\rangle \exp(-t_0\Lambda_n)\langle q^{(n)}|p_0\rangle, \qquad (4)$$

where $\langle q^{(n)}|$ and $|p^{(n)}\rangle$ are the left and right eigenvectors of the matrix M_χ, Λ_n are the eigenvalues of M_χ and $\langle q_0|$, $|p_0\rangle$ are the eigenvectors corresponding to the lowest eigenvalue $\Lambda_{\min}$. The cumulants generated from the CGF in Eq. (4) will in general be a function of t_0.

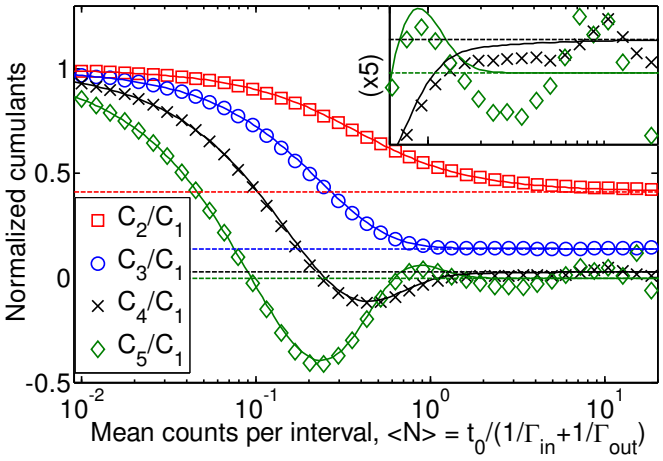

FIG. 3: Normalized cumulants evaluated for different lengths of the time interval t_0. The symbols show the experimental data, extracted from a time trace of length $T = 10$ minutes, containing 350595 events, with $a = 0.053$, and $\Gamma_{\rm tot} = 3062$ Hz. The solid lines are calculations from the FCS given by Eq. (4) in the text, while the dashed lines are the asymptotes for $t_0 \to \infty$. The inset shows a magnification of the vertical axis (horizontal axis unchanged) for C_4/C_1 and C_5/C_1 for $\langle N\rangle > 0.6$.

To investigate how small t_0 can be before systematic errors become relevant, we calculate the cumulants from the CGF of Eq. (4) with the master equation matrix M_χ of Eq. (1). The results are shown in Fig. 3, where we plot the normalized cumulants as a function of the mean number of counts per interval, $\langle N\rangle = t_0/(1/\Gamma_{\rm in}+1/\Gamma_{\rm out})$. The symbols show cumulants extracted from measured data ($T = 10$ minutes, $a = 0.053$, $\Gamma_{\rm in} + \Gamma_{\rm out} = 3062$ Hz and $\Gamma_{\rm det} = 14$ kHz), while the solid lines are results from the CGF for the same set of parameters. The dashed lines are the asymptotes for the limiting case $t_0 \to \infty$.

In general, the data and the theory are in good agreement. There are some deviations in the fourth and fifth cumulants for large t_0 ($\langle N\rangle > 6$ in Fig. 3), but these are statistical errors due to the shortness of the total time trace. For short t_0, all cumulants converge to $C_n/C_1 \to 1$. This is because as $\langle N\rangle \ll 1$, the probability distribution $p_{t_0}(N)$ will be non-zero only for $N = 0$ and $N = 1$, with $p_{t_0}(0) = 1-q$, $p_{t_0}(1) = q$ and $q = \langle N\rangle$. This is the definition of a Bernoulli distribution, for which the normalized cumulants $C_n/C_1 \to 1$ as $q \to 0$ [24].

Focusing on the other regime, $\langle N\rangle > 1$, we see that cumulants of different orders converge to their asymptotic limits for different values of t_0. The second cumulant needs a longer interval t_0 to reach a specified tolerance compared to the higher cumulants. This is of interest for the experimental determination of higher cumulants. By choosing a shorter value of t_0 when calculating higher cumulants, the amount of samples $m = T/t_0$ can be increased. For the data in Fig. 1, the cumulants were calculated with intervals t_0 giving $\langle N\rangle = 15$ for C_2, $\langle N\rangle = 6$ for C_3, $\langle N\rangle = 3$ for C_4 and $\langle N\rangle = 2$ for C_5. The maximal deviations between the correct cumulants and the ones determined with a finite length t_0 can be estimated by checking the convergence for all values of the asymmetry. For the data shown in Fig. 1, we find $\Delta C_2/C_1 = 0.007$, $\Delta C_3/C_1 = 0.009$, $\Delta C_4/C_1 = 0.01$ and $\Delta C_5/C_1 = 0.03$.

Coming back to the results of Fig. 1, we are now able explain why the measured cumulants show lower values compared to the perfect-detector theory. The dashed lines in Fig. 1 are the cumulants calculated from the combined QD-detector model of Eq. (1), with $\Gamma_{\rm det} = 14$ kHz. The overall agreement is good, especially since no fitting parameters are involved. Higher cumulants end up to be slightly lower than theory predicts. We speculate that the deviations could be due to low-frequency fluctuations of the tunneling rates over the time of measurement.

In conclusion, we have measured the first five cumulants of the distribution of charge transmitted through a QD. The ability to measure higher cumulants shows that we can determine the distribution function very precisely. The high accuracy of the technique makes it a promising tool for probing subtle effects in the transport statistics of more complex QD systems. We have found that the measured statistics depends strongly on the bandwidth of the charge detector. By including the detector in the model, we show that the framework of FCS can be used to predict noise levels for systems with a finite bandwidth detector. The principle is general and can be applied to any rate-equation model used for calculating the FCS. Financial support by the NCCR Nanoscience through the Swiss Science Foundation (Schweizerischer Nationalfonds) is gratefully acknowledged.

[1] Y. M. Blanter and M. Büttiker, Physics Reports **336**, 1 (2000).

[2] L. S. Levitov, H. W. Lee, and G. B. Lesovik, J. Math. Phys. **37**, 4845 (1996).

[3] T. Fujisawa, T. Hayashi, R. Tomita, and Y. Hirayama, Science **312**, 1634 (2006).

[4] L. S. Levitov and M. Reznikov, Phys. Rev. B **70**, 115305 (2004).

[5] D. Bagrets, Y. Utsumi, D. Golubev, and G. Schön, Fortschritte der Physik 54, 917-938 (2006). **54**, 917 (2006).

[6] W. Belzig, Phys. Rev. B **71**, 161301(R) (2005).

[7] D. Loss and E. V. Sukhorukov, Phys. Rev. Lett. **84**, 1035 (2000).

[8] D. S. Saraga and D. Loss, Phys. Rev. Lett. **90**, 166803 (2003).

[9] B. Reulet, J. Senzier, and D. E. Prober, Phys. Rev. Lett. **91**, 196601 (2003); Y. Bomze *et al.*, Phys. Rev. Lett. **95**, 176601 (2005).

[10] S. Gustavsson, R. Leturcq, B. Simovic, R. Schleser, T. Ihn, P. Studerus, K. Ensslin, D. C. Driscoll, and A. C. Gossard, Phys. Rev. Lett. **96**, 076605 (2006).

[11] S. Gustavsson, R. Leturcq, B. Simovic, R. Schleser, P. Studerus, T. Ihn, K. Ensslin, D. C. Driscoll, and A. C. Gossard, Phys. Rev. B **74**, 195305 (2006).

[12] L. Mandel and E. Wolf, *Optical Coherence and Quantum Optics* (Cambridge University Press, 1995).

[13] W. Lu, Z. Ji, L. Pfeiffer, K. W. West, and A. J. Rimberg, Nature **423**, 422 (2003).

[14] T. Fujisawa, T. Hayashi, Y. Hirayama, H. D. Cheong, and Y. H. Jeong, Appl. Phys. Lett. **84**, 2343 (2004).

[15] J. Bylander, T. Duty, and P. Delsing, Nature **434**, 361 (2005).

[16] M. Field, C. G. Smith, M. Pepper, D. A. Ritchie, J. E. F. Frost, G. A. C. Jones, and D. G. Hasko, Phys. Rev. Lett. **70**, 1311 (1993).

[17] A. Fuhrer, A. Dorn, S. Lüscher, T. Heinzel, K. Ensslin, W. Wegscheider, and M. Bichler, Superl. and Microstruc. **31**, 19 (2002).

[18] L. P. Kouwenhoven, C. M. Marcus, P. M. McEuen, S. Tarucha, R. M. Westervelt, and N. S. Wingreen, in *Mesoscopic Electron Transport*, edited by L. L. Sohn, L. P. Kouwenhoven, and G. Schön (Kluwer, Dordrecht, 1997), NATO ASI Ser. E 345, pp. 105–214.

[19] R. Schleser, E. Ruh, T. Ihn, K. Ensslin, D. C. Driscoll, and A. C. Gossard, Appl. Phys. Lett. **85**, 2005 (2004).

[20] L. M. K. Vandersypen, J. M. Elzerman, R. N. Schouten, L. H. Willems van Beveren, R. Hanson, and L. P. Kouwenhoven, Appl. Phys. Lett. **85**, 4394 (2004).

[21] D. A. Bagrets and Y. V. Nazarov, Phys. Rev. B **67**, 085316 (2003).

[22] O. Naaman and J. Aumentado, Phys. Rev. Lett. **96**, 100201 (2006).

[23] C. E. Shannon, Proc. Institute of Radio Engineers **37**, 10 (1949).

[24] E. W. Weisstein, "Bernoulli Distribution." From MathWorld - A Wolfram Web Resource. http://mathworld.wolfram.com/BernoulliDistribution.html.